R. T. Lynch, Jr. M. B. Small R. Y. Hung

GaAs/(GaAl)As Laser Technology

This paper is a review of some recent work at IBM on semiconductor injection lasers. An automated system has been built and used for the epitaxial growth of laser material and we describe testing procedures used to characterize this material. Results on the degradation of these lasers at high continuous wave optical power are also presented.

Introduction

In 1962, feverish activity at several laboratories around the world was concentrated on obtaining lasing action in a semiconductor material. This work resulted in nearly simultaneous reports of the observation of lasing in GaAs by three groups, including one at IBM [1-3].

The first GaAs lasing structures with diffused p-n junctions operated only at low temperature and very high currents. Refinements in materials and structures over the years have led to present-day semiconductor lasers that operate continuous wave (cw) at room temperature and can produce milliwatts of coherent light at currents as low as tens of milliamperes. Among the most important of these refinements was the introduction of heterojunctions, which use materials with different bandgaps to help confine the carriers until they can recombine. Though proposed in 1963 [4], this refinement was not implemented until liquid phase epitaxy (LPE) techniques were introduced [5] and used to grow lattice-matched layers of GaAs and (GaAl)As [6]. This resulted in the development of low-threshold, room-temperature cw double heterostructure (DH) lasers in 1970 [7, 8]. Combined with a mechanism for confining the current to a small stripe through the junction [9-11], the DH structure is now standard for room-temperature cw injection lasers.

In addition to well-known applications in optical fiber communications [12], injection lasers are used in several other areas, including optical memory [13], video disk [14, 15], and liquid crystal display [16] systems. Each application puts its own set of constraints on the properties

and performance of injection lasers. For example, optical communications systems operate at low power but require high-speed modulation and long lifetimes, whereas display applications require a high average optical power but significantly less stringent lifetime performance.

Since 1970 a major thrust of research has been toward improving the reliability of stripe-geometry DH lasers. Some important degradation mechanisms have been identified [17-19] and operating lifetimes of decades are now predicted for lasers used in optical communications systems [20]. The maturity of the field is indicated by the recent appearance of two textbooks devoted primarily to heterostructure lasers [21, 22].

In spite of advances in the basic understanding of lasing in semiconductors, it is still difficult to reproducibly manufacture DH lasers with uniformly excellent properties and lifetimes. Until this is done routinely in a manufacturing environment, many potential applications will not be fully realized. Recent work at IBM on the technology of GaAs/(GaAl)As DH semiconductor injection lasers has included investigation of automating many of the routine but delicate tasks associated with their manufacture and testing. After a brief explanation of the principles of DH lasers, we present a description of this work. The growth of laser material, including the use of an automated LPE system, is discussed. This automation, along with various improvements in equipment and techniques, removes much of the previously observed variation in quality among growth runs. Fabrication and packaging steps are

Copyright 1979 by International Business Machines Corporation. Copying is permitted without payment of royalty provided that (1) each reproduction is done without alteration and (2) the *Journal* reference and IBM copyright notice are included on the first page. The title and abstract may be used without further permission in computer-based and other information-service systems. Permission to *republish* other excerpts should be obtained from the Editor.

585

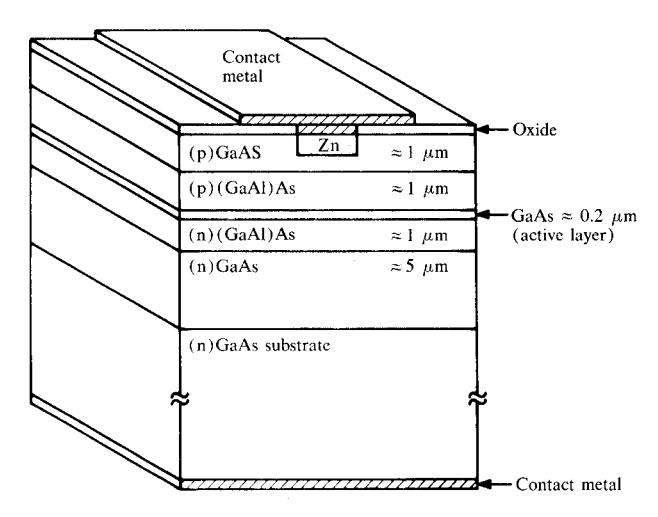


Figure 1 Double heterostructure laser with oxide-defined current stripe. The active layer may be either pure GaAs or GaAs containing a small amount (5-10%) of Al.

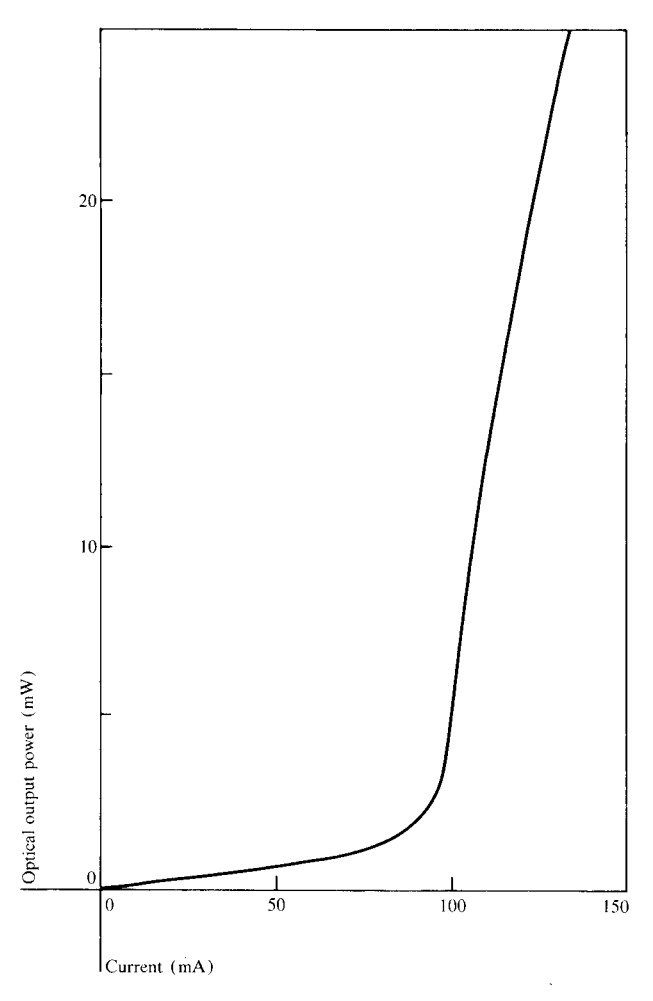


Figure 2 Laser optical output as a function of injection current.

also briefly outlined; these have not been automated. We then describe various tests performed on the packaged laser devices. The more routine tests are made with the aid of a computer data acquisition system. Finally, we present the results of aging experiments, where we are particularly concerned with laser reliability at relatively high cw output power.

Figure 1 shows the structure of a stripe-geometry DH laser consisting of several epitaxial layers grown on GaAs substrates. The actual lasing occurs in the thin active layer, which may be either pure GaAs or GaAs containing a small amount (5-10%) of Al. The layers on either side of this active layer form the heterojunctions. The final layer of GaAs and a surface layer of zinc diffused through the oxide stripes are used to make electrical contact. In a variation on this structure, the top GaAs layer is doped n-type, rather than p-type (as shown). In this case, a channel of zinc is diffused all the way through this n-type layer to form a narrow current path. This reduces the amount of lateral current spread and improves the laser performance [23]. These two structures are referred to as oxide-stripe and diffused-stripe lasers, respectively.

Electrons and holes are injected from the wide-bandgap Ga_{0.65}Al_{0.35}As layers into the Ga_{0.9}Al_{0.1}As active layer. Because of potential barriers at the heterojunctions, the carriers are forced to remain together in the thin active layer until they can recombine and emit light. The wide-bandgap regions have a smaller refractive index than the active layer, and thus act as a waveguide for the light. Cleaved facets at each end of the laser form feedback mirrors. Because the current flows in a narrow stripe through the active layer, the injected carrier distribution has a peaked profile; this results in an effective lateral index profile. The light thus propagates in a three-dimensional cavity formed by this gain-guiding, by the index step at the heterojunctions, and by the facet mirrors.

The carrier population in the active layer can be inverted when the injection current is high enough, and the device begins lasing when the resulting gain exceeds the net losses, including the light escaping from the end facets. Above this threshold current, the extra carriers injected mainly contribute to the light intensity. There are, however, competing recombination processes as well as free carrier absorption of the light, so the incremental efficiency above threshold is approximately one photon for every two or three injected electron-hole pairs. The net result can be seen in Fig. 2, which is a graph of optical output vs current. The sharp threshold phenomenon is evident, with a steep increase in emission above threshold. The slope of this line is the differential quantum efficiency.

Reproducible growth of double heterostructure laser material

Semiconductor multilayer heterostructures may be grown by a number of epitaxial processes: liquid phase epitaxy (LPE), molecular beam epitaxy (MBE) or chemical vapor deposition (CVD). For the growth of lasers LPE is at present the most commonly used process. One reason for this is that material grown by the LPE process generally has a higher luminescent efficiency than that produced by the other processes [24, 25]. Another reason is that (GaAl)As cannot be grown by the conventional halide process for CVD because of the reactivity of Al with oxygen, which causes the Al vapor to react with the glass envelope [26]. More recently, development of the metalorganic process has made it possible to grow this alloy by CVD [27]; this process has practical advantages over LPE, and is likely to become more important if it can produce lasers of equivalent quality. Molecular beam epitaxy has also been used to produce lasers (cf. Ref. [28]); it has some potential advantages over LPE and CVD in the control it offers in the growth of very thin layers. Nevertheless. LPE remains at present the main method for laser fabrication. Our discussion is particularly directed toward procedures and equipment which provide good control over the compositions, dimensions, and crystal quality of the material grown.

• Compositional considerations

Liquid phase epitaxy is a solution growth process in which a series of layers of defined compositions can be grown from a sequence of cooling solutions in a single operation. Figure 3 illustrates the arrangement by which a series of solutions may be presented to the substrate. The process of growth may be understood by considering the phase diagram of the GaAs system (Fig. 4). Solid GaAs can exist in equilibrium with a range of liquidus compositions. When Ga-rich compositions are used, the equilibrium vapor pressure of As is lower (simplifying practical problems) and the material produced has a higher luminescent efficiency. To grow a layer, one prepares a solution of composition C_0 at temperature T_0 . A GaAs substrate inserted into such a solution is in equilibrium with it. When the system is cooled, the solution becomes supersaturated and growth takes place on the substrate. Discounting any unintentional components, the solutions usually have four major components: Ga, Al, As, and a dopant. The dopants generally do not have a marked effect on the liquidus and solidus surfaces. If their effects are neglected, it is only necessary to consider a ternary system. Figure 5 shows the solvent (Ga)-rich corner of a section through the ternary phase diagram at temperature $T_{\rm o}$. By defining the composition of the required solid and the temperature for growth, the composition of the equilibrium liquid is fixed. It is fortunate that the physical

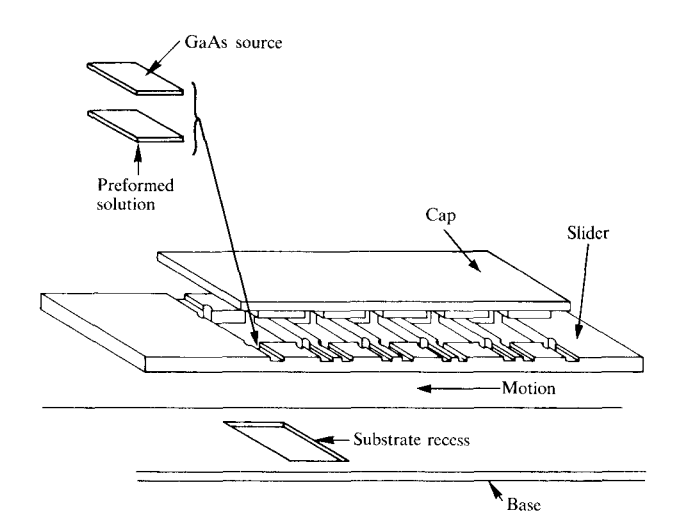


Figure 3 Schematic view of the growth crucible.

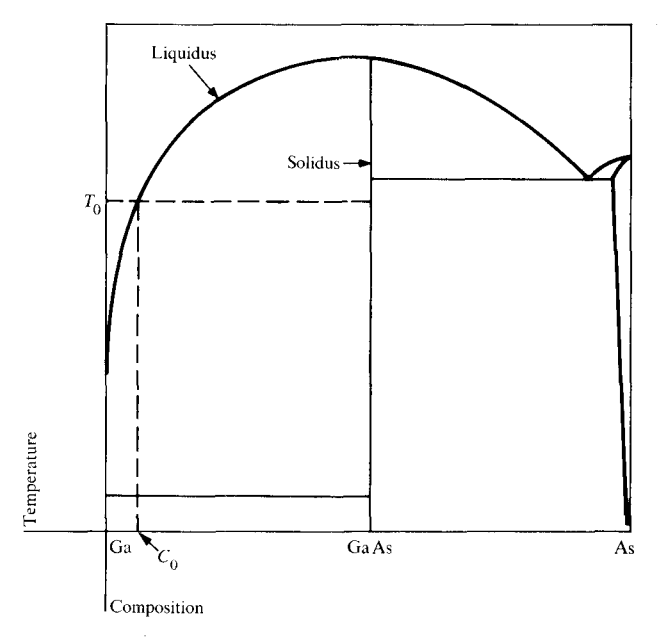


Figure 4 Phase diagram of the GaAs system.

chemistry of this type of system is well enough understood to allow the phase diagram to be calculated and that the necessary thermodynamic data are available [29]. Thus, one may in principle compute the necessary compositions of each of the solutions.

In practice, however, such computations would require extremely accurate monitoring of the temperature at which the growth of each layer starts and metering of the

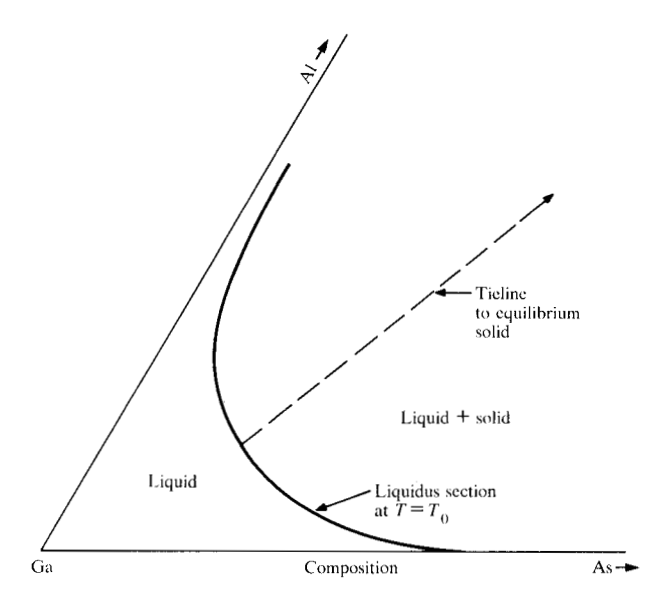


Figure 5 Section through the (GaAl)As ternary phase diagram at temperature $T_{\rm a}$.

compositions of the solutions. Rather than depending on this computation, one normally uses a sacrificial substrate to which each solution is exposed prior to the main substrate, thus allowing the lower surfaces of the solutions to come to equilibrium with the solid phase. Although this offers some control, the overall composition of the solution is a function of this boundary condition, the remote boundary condition, transport processes, and the time spent on the sacrificial wafer. The time involved depends on the time required for the growth of the preceding layer and so may be different for each solution. Better control is achieved if the equilibrium solid is continually in contact with the upper surface of each solution and the main substrate is introduced to the lower surfaces of each in turn. Originally the solutions are prepared with only the necessary Ga, Al, and dopant. A wafer of polycrystalline GaAs is then placed on the upper surface. Prior to the growth sequence the solution is equilibrated with this solid phase. Sufficient solid dissolves to saturate the solution, and the surface of the solid in contact with the solution takes the equilibrium composition.

This procedure eliminates the necessity for very precise weighing and has certain other advantages. The crucible in which the solutions are contained is made of graphite. Although the solutions wet the substrates, they do not wet graphite, making difficult the complete removal of solutions from the substrate. Any solution mixing which may result from this not only alters the composition of the next layer, but also its thickness [30]. Providing a wetted solid surface to form the upper part of the

container for each solution reduces this problem. A further advantage is that the compositions of all solutions may be controlled at all times. During the cooling phase, the lower surface of each solution, normally on a neutral surface (graphite), is supersaturated by an amount dependent upon the cooling rate, the dimensions of the solution, and the transport processes in the solution. This supersaturation is present when the solution is presented to the main substrate and allows control over the nucleation of each layer [31]. It also prevents dissolution of one layer of a heterostructure by the next solution. Even though the solution may be exactly saturated, it cannot be in equilibrium with a solid layer which has just grown in the previous, different solution. In approaching equilibrium either dissolution or growth may occur. The very thin active layer of the laser, for instance, tends to dissolve in the succeeding solution unless it is supersaturated [32].

Apart from the overall compositions of the solutions, a major factor controlling the growth rate of each layer is the transport of material through the solutions, which may take place either by diffusion or by a mixture of diffusion and convection. The horizontal-rotating-disk process, which is used to grow epitaxial layers for magnetic bubble applications [33], uses the fluid motion produced by the rotation to obtain a well-defined transport process. To bypass the engineering problems of applying this technique to a series of solutions that are very susceptible to oxidation, it is usual to obtain control over the transport processes in this system by making the solutions quiescent.

Any horizontal density gradients in a fluid cause "natural" convection, while vertical gradients may be either stabilizing or destabilizing. The latter cause convection only if the critical Rayleigh number for the solution is exceeded. In our geometry the growth process takes place on horizontal surfaces, thus producing vertical density gradients. By making the solution thin enough (≈ 1.5 mm), we ensure that the critical Rayleigh number is not exceeded [34]. Also, since the solutions as a whole are close to equilibrium, any naturally occurring convection does not have a great effect on the growth rate.

A further advantage of using thin solutions is that the growth rate is essentially constant over the major period of the growth of each layer. This makes the control of thickness easier and provides control over those aspects of growth morphology that are functions of rate [35]. Both the Arrhenius nature of the solubility curves and the transient nature of the concentration profiles in the solutions may contribute to transient growth rates. Provided the solutions are made thin enough that the growth period is long compared to the diffusion relaxation time, the con-

centration profiles have a constant shape for most of the period. If at the same time the requisite layer thickness may be produced over a small temperature range, the growth rate is essentially constant. A detailed analysis [36] has described conditions under which the growth rate is essentially constant for all layers but the active layer.

◆ Crystal quality

Crystal quality is important for a good yield of long-lived lasers. Dislocations threading through the active layer of a device lead to the development of large networks of dislocations during the operation and subsequent degradation of the device. Some of these dislocations originate in the substrate. However, substrates are obtainable with a sufficiently low density of these defects to provide a high yield of long-lived lasers. During the epitaxial growth process it is important not to produce a greater density of dislocations than that present in the substrate; this may occur if solid impurity particles are included in the growing layer. If small, these particles have been shown to result in complex dislocation networks [37]; if large, they can result in local discontinuities in the growth of subsequent layers [38]. This can be a particular problem with thin solutions. The hydrostatic pressure is not sufficient to overcome surface tension and force the solutions against the walls of their enclosures. Under these conditions, particles on the surfaces of the solutions (most likely either aluminum oxide or graphite) tend to transfer to the surface of the substrate during interchange.

Figure 3 illustrates the design of a crucible that substantially reduces the number of particles transferred to the surface of the wafer. By pushing some excess solution up columns in the corners of each of the containers, a higher hydrostatic pressure is produced at the bottoms of the thin solutions. The corners of each compartment have been drilled out so that they both contain this solution and provide a radius that can be filled by the solution under this pressure. The pressure is limited by the total thickness of the sliding piece, while the thickness of the solution is determined by the penetration of the projections on the cap into the sliding piece.

The incidence of oxide particles may be reduced by baking the solutions in hydrogen prior to use [39]. We have devised a process for performing this operation with bulk solutions, which may be subsequently divided into defined melt volumes. The crucible used (see Fig. 6) consists of a number of interleaved sections, each of the desired thickness for one unit of solution. When the interleaved sections are in one alignment, each of the compartments in a single leaf is part of a large compartment formed by the multiple leaves. A different bulk solution may be placed in each of these. At this stage the Al

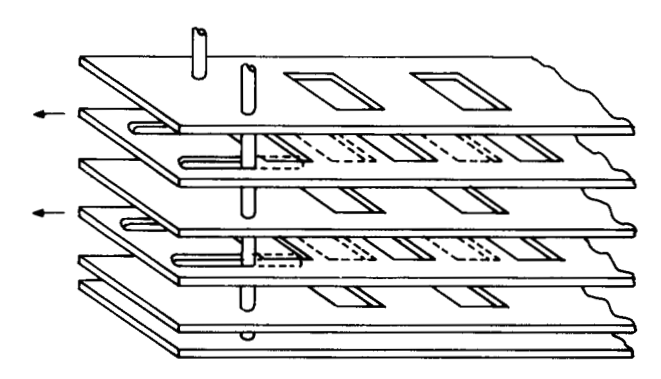


Figure 6 Design of crucible for making solution preforms.

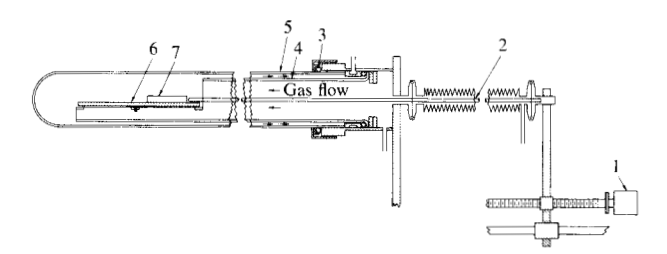


Figure 7 Apparatus for holding and manipulating the crucible: 1, stepping motor; 2, push-rod; 3, sealing O-ring; 4, cantilevered silica support; 5, outer silica envelope; 6, carbon boat base; and 7, carbon boat slider.

needed to make up the solution is placed in a separate slider adjacent to the top of the solution to which it is to be added. The solutions are then baked in hydrogen for 24 hours to reduce oxides of gallium. The Al is then added and the solutions allowed to homogenize for 16 hours. By sliding one set of alternate interleaved sections relative to the others, a number of exact solution volumes are defined. The whole system is then cooled to freeze the solutions before they are unloaded and stored in an inert atmosphere. This procedure has eliminated many of the problems associated with the weighing and handling of individual solutions.

• Growth enclosure and automation

The growth enclosure has been designed to ensure that the manual operation of loading crucibles into it is both easy to perform and reproducible. From this stage the growth process has been automated, improving control over the timing of each process and the positioning of each solution relative to the wafer.

Figure 7 illustrates the construction of the enclosure. The major points of difference between this and conventional systems are as follows:

•The crucible is supported on a cantilevered table, making it more readily accessible than if it had to be in-

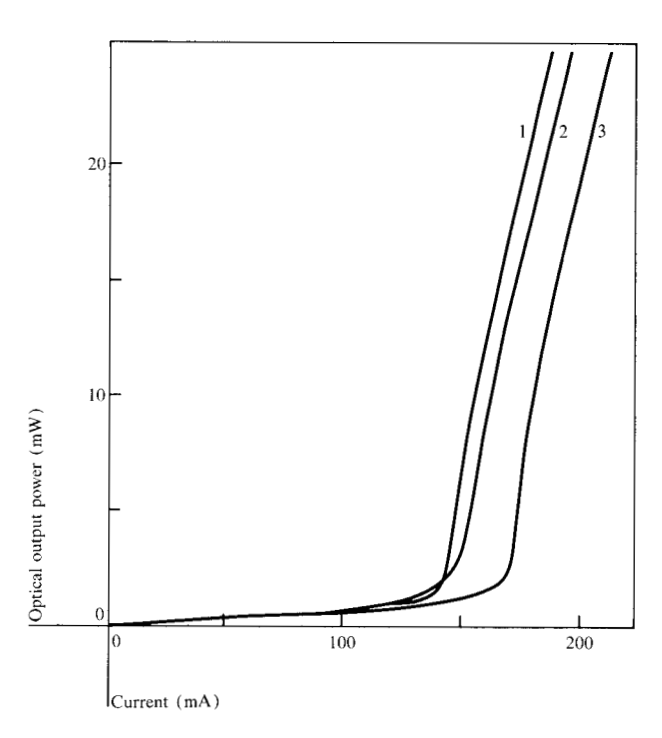


Figure 8 Power-current curves obtained using automatic testing apparatus: curve 1, 25°C pulsed, curve 2, 25°C cw, curve 3, 50°C pulsed; 380-µm cavity length.

serted into a tube. Once it is placed on the cantilever, the surrounding envelope may be brought around it. Two pins in the bottom of the crucible line up with holes in the base to ensure reproducible positioning.

- A single O-ring seal is used to gain access to the system, reducing the likelihood of introducing leaks.
- The motion of the slider is controlled by a stepping motor. This manipulates a push-rod through a bellows seal rather than a sliding seal. The latter eliminates any possibility of leaks due to manipulation, while the former provides excellent positional control. It also allows the process to be automated.

The operations necessary to grow the desired structure are regulated by a sequence controller. A timer is started when the temperature of the crucible reaches a preset equilibration temperature. Sufficient time is then allowed for the solutions to homogenize. Following this, the furnace is programmed to cool at a relatively fast rate prior to the introduction of the first solution to the substrate. This provides a greater supersaturation for the growth of the first layer on the substrate than is used for subsequent layers, which are nucleated on freshly grown surfaces. The sequence controller determines the period spent by each solution on the wafer and regulates the distance the slider is moved at each stage. When the final solution is removed, the furnace is simultaneously rolled away from the growth enclosure.

With these procedures it has become possible for us to grow in one day (using a single furnace) sufficient material to fabricate a thousand lasers. Since these procedures have been adopted, reproducibility from wafer to wafer has increased considerably. The reproducibility of the final product is, of course, a function of the entire manufacturing process, including, in addition to crystal growth, fabrication and packaging steps.

Fabrication and packaging

The multilayer structure produced by the LPE process gives good carrier confinement in the direction normal to the layers. However, some means must be provided for lateral current confinement. Many methods of stripe definition have been used to obtain this confinement [9–11]. Highly resistive areas can be formed using proton [10] or oxygen ion [11] bombardment; stripes of undamaged material then form the current paths. The simplest method is to etch stripes in a layer of oxide deposited on the top epitaxial layer [9]. In this case, the current flows only through the oxide-free stripes, and is restrained from spreading laterally by the resistivity of the thin top layers.

The fabrication process starts with a thorough cleaning of the wafer surface. An ≈100-nm Al₂O₂ layer is deposited on the wafer to serve as a mask for the subsequent zinc diffusion. A stripe 15 μ m wide is opened in the oxide by standard photolithography techniques. Zinc diffusion is carried out in a closed tube with ZnAs, as the diffusion source to achieve a shallow p+ layer with high surface concentration ($\approx 10^{20} \text{ cm}^{-3}$) so that a low-resistance ohmic contact can be reproducibly made to it. For the diffusedstripe lasers, the Zn must penetrate through the n-type GaAs cap layer. The wafers are initially about 250 μ m thick and it is necessary to thin the wafer down by mechanical lapping to $\approx 100 \mu m$ for ease in the later cleavage process. The thinning step also removes the p⁺ diffused region from the n substrate. The n-side and p-side ohmic contacts are formed by Au-Ge-Ni alloy and Ti-Pd-Au multilayer vacuum evaporations, respectively, along with appropriate alloving steps. These materials not only form an intimate contact with the GaAs substrate and cap layers, but also serve as part of the bonding material when the laser chips are packaged. Processed wafers are cleaved into bars, each containing many lasers. Optical power output P vs current I curves are taken under shortpulse conditions for all lasers on the bars. The output wavelength is also measured for several units on each bar, permitting us to identify the better wafers. Lasers from these wafers are then separated into individual chips. The next fabrication step, packaging the laser on a heat sink, is a crucial one because of the amount of heat generated locally by the large current densities at which these devices operate. To achieve the most effective path

for heat dissipation, the laser chip is indium soldered to a copper heat sink with the epitaxial side down. Special care is taken to minimize the mechanical stress on the chips during the bonding process. It has been generally recognized that In, because it is soft and has a low eutectic temperature with gold, is a desirable bonding material; however, a recent report suggests that Au-Sn may be better [40].

Many applications of GaAs lasers require that the light be guided through optical fibers. An etched silicon plate has been developed as a substrate for the laser chip and optical fiber [41]. This silicon "miniature optical bench" allows precise positioning and alignment of the laser, output fiber, and a cylindrical lens in one integrated package.

Testing and characterization

Initial testing of the packaged lasers is done with automated test equipment controlled by a host computer. Six packaged lasers are mounted in front of a large-area Si photodetector. Power vs current curves are run automatically under both pulsed (curve 1 in Fig. 8) and cw (curve 2) conditions at 25°C, and values of optical power, current, and voltage across the lasers are recorded. From these digitized curves the threshold current, differential quantum efficiency, and electrical series resistance are calculated. A second pulsed P-I curve is run at a higher temperature (50°C, curve 3), and from the three curves the thermal resistance and temperature dependence of threshold are determined.

The values obtained for these parameters give useful information about the material properties and the packaging quality. Threshold current density is a commonly used indicator of bulk-material quality, although its dependence on various other parameters such as cavity length and active layer thickness also needs to be accounted for. The lasing wavelength is useful as a check of the aluminum content in the active layer. Thermal resistance is largely determined by the quality of the bond between the laser chip and the heat sink [42, 43]; it is an important quantity because it influences the difference between pulsed and cw threshold currents. The temperature rise in the active layer and the temperature profile resulting from cw operation are both detrimental to efficient lasing [44]. The curves shown in Fig. 8 are typical of results for well-bonded lasers. For this unit the temperature rise is a few degrees, and the threshold increases about 20% between 25 and 50°C.

In addition to initial tests on all lasers packaged, a few lasers from each batch are selected to undergo further characterization tests, including measurements of nearand far-field stimulated emission patterns and injected

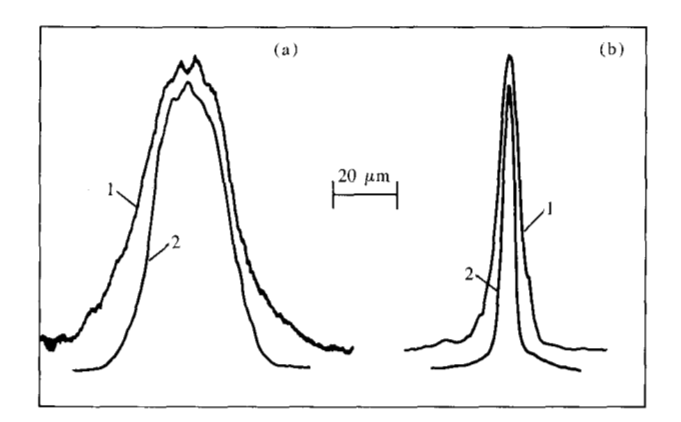


Figure 9 (a) Near-field scans of spontaneous output vs distance along active layer for oxide-stripe (curve 1) and diffused-stripe (curve 2) structures. (b) Similar profiles of lasing intensity; curves 1 and 2 as in (a).

current profiles. We obtain the latter by observing the spontaneous emission near-field pattern using a 780-nm bandpass filter. The emission at this wavelength is strongly absorbed by the laser material; thus, only light from very near the output facet is detected. The resulting optical intensity pattern closely follows the current profile across the stripe region. The near-field profiles are obtained by imaging the output facet on the detector of an optical multichannel analyzer. This allows the entire profile to be observed on an oscilloscope display. This is distinctly superior to imaging the pattern on a slit because subtle interactions of the gain-guided lateral modes can be more easily observed as the current level is changed. Spectra are also recorded with sufficient resolution to distinguish the number and relative intensities of the longitudinal modes of the cavity.

We have carefully compared the operating characteristics, both electrical and optical, of oxide-stripe and diffused-stripe lasers. The examples given below are representative of results we have obtained by comparing good units from each of several high-quality wafers of both kinds. Curves 1 and 2 in Fig. 9(a) show the spontaneous emission near-field profiles at 780 nm for an oxide-stripe and a diffused-stripe laser, respectively. These are essentially profiles of the excess carrier concentration in the active layer. For the undoped or lightly Si-doped active layers in these lasers, they are also similar to the gain profiles [45]. The efficacy of the extra current confinement in the diffused-stripe structure is evidenced by the narrower profile for that laser. Allowing for carrier diffusion in the active layer, these profiles imply that the current spread is small in the diffused-stripe laser compared to a spread of about 6 µm in the oxide-stripe unit.

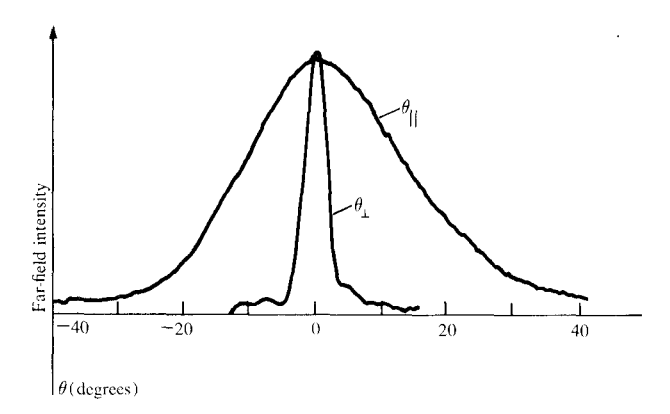


Figure 10 Far-field scans of lasing intensity vs angles parallel to and perpendicular to the junction plane, θ_0 and θ_1 , respectively.

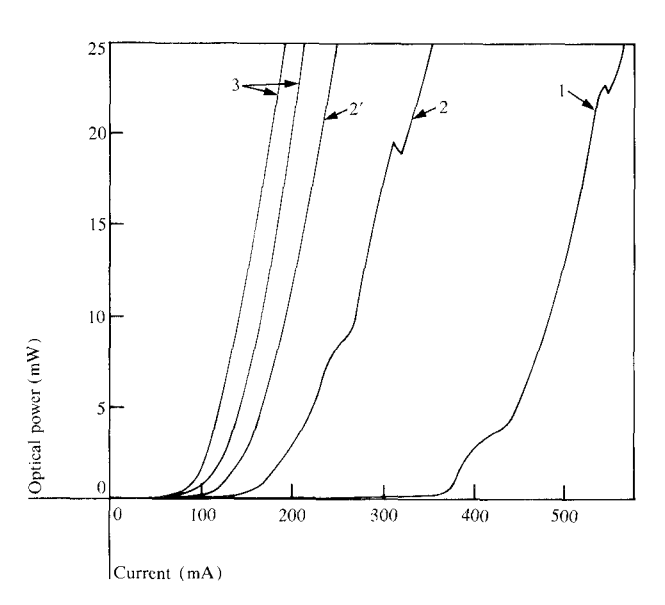


Figure 11 Optical power vs current curves for a long cavity laser (curve 1); two (long and short) pieces made by cleaving this laser (curves 2 and 2', respectively); and two pieces made by cleaving the long piece above (curves 3). Note the change in the strong kink at 2-3 mW in curve 1. Curves for the final three pieces (2' and 3) are quite linear to above 25 mW.

This results in a 30% reduction in threshold current density for the diffused-stripe laser. Further reduction in threshold could be accomplished by reducing the carrier diffusion length in the active layer, perhaps by means of proton [10] or oxygen [11] bombardment through the active layer, or a mesa structure [46] of some kind. However, the existence of a damaged region or etched surface so close to the recombination region is suspected to be detrimental to laser lifetime [47].

Curves 1 and 2 in Fig. 9(b) compare the near-field lasing profiles for oxide- and diffused-stripe lasers, respectively. In general, the widths of these profiles fall in the same range for the two types of structures. A significant difference is seen when the mode behavior is observed as a function of current. The oxide-stripe units show a more pronounced tendency for the near-field lasing profile to shift among several lateral modes. This can be attributed to a flatter gain profile compared to that in diffused-stripe devices. Far-field intensity patterns have also been studied. Angular scans parallel to the junction plane (θ_{\parallel} in Fig. 10) give information similar to that contained in near-field patterns. The widths of far-field scans perpendicular to the junction (θ_{\perp} in Fig. 10) are related to the thickness of the active layer and index step at the heterojunctions.

Longitudinal-mode spectra generally show that most of the lasing output is concentrated in one or a few modes when the lateral mode is either fundamental or at least has a stable pattern vs current. When this is not the case, the spectra usually contain a dozen or more longitudinal modes.

We have observed an interesting dependence of the severity and position of kinks in *P-I* curves on the cavity length in these laser structures. Long cavities tend to allow strong kinks to appear at relatively low output powers. Cleaving the same lasers to shorter cavity lengths results in the kinks moving to higher optical power and in general becoming less severe [48] (see curves 1-3 in Fig. 11). Detailed examination of near-field lasing patterns suggests an explanation for this observation in terms of the relative ability of higher-order lateral modes to compete for the available gain in long- vs short-cavity lasers [48].

Reliability

Applications that use semiconductor lasers as heat sources generally must operate at fairly high optical power compared to that used in optical communications systems. Writing on a video disk is usually done with very high peak power, short pulses. Liquid crystal display cells have been built that require tens of milliwatts of laser output for reasonable writing speeds [16]. Reliability under high-power pulse operation is mostly concerned with sudden catastrophic damage to the laser facets resulting from the very large optical field strengths [49]. Lifetimes under low-power (2- to 5-mW) cw operation are so long that aging experiments are normally carried out at elevated temperatures in order to accelerate the degradation [50, 51]. The lifetime performances of DH lasers run at high cw optical power have received less attention [52-54].

An early experiment was run to estimate any increase in the degradation rate as the optical power is raised. We aged a set of lasers under constant current conditions, with the heat sink temperature alternating periodically between 25 and 50°C. The aging currents chosen were those required initially to reach 25 mW at 25°C. During the experiment, the optical output of the lasers averaged about 10 mW at the higher and 22 mW at the lower temperatures used. Each temperature condition was maintained long enough (500-1000 hours) to allow a degradation rate to be established. In Fig. 12 we display the current required to reach 25 mW at 25°C (solid lines) as a function of aging time. In an operational sense, this is clearly the most useful parameter for monitoring degradation because it points out the actual useful lifetime of a device under contemplated operating conditions. (Other possible monitoring parameters are often relatively insensitive to some important degradation mechanisms. For example, pulse threshold current values have been used to monitor bulk-material changes during aging [55, 56] precisely because this parameter is insensitive to bond degradation.) The results of this experiment show that there is little difference between the degradation rates observed under the two conditions used. For these lasers, the degradation induced by higher-power operation (22 vs 10 mW) is just offset by the reduction in temperature (25 vs 50°C). If the generally observed temperature acceleration factor [50] is used, this result implies that the degradation at 22 mW is an order of magnitude faster than that at 10 mW.

In the rest of this section we give results of room-temperature aging of diffused-stripe lasers at high cw optical power (20 mW). This experiment was intended as a study of the feasibility of using standard cw semiconductor lasers in applications requiring this kind of output. For this initial investigation no attempt was made to optimize the laser structure for 20-mW cw operation. The lasers, which had uncoated facets, were aged in a dry nitrogen environment, with the heat sinks controlled at 25°C. The optical output was monitored, and when a significant change occurred, or at appropriate intervals, the lasers were tested by running pulsed and cw *P-I* curves.

A set of diffused-stripe lasers was selected from several wafers for aging under these high-power conditions. After 20 hours of aging, screening criteria developed from earlier oxide-stripe laser aging data were applied. Fifteen units were identified at this time as meeting the criteria, although all the lasers continued on the life test. Figure 13 shows the lifetime τ_{ℓ} distribution of these fifteen units on a log normal graph. A significant effect of using the screening procedure is a large reduction in the standard deviation of the lifetime distribution. This is important because often the key reliability figure for a set of lasers is

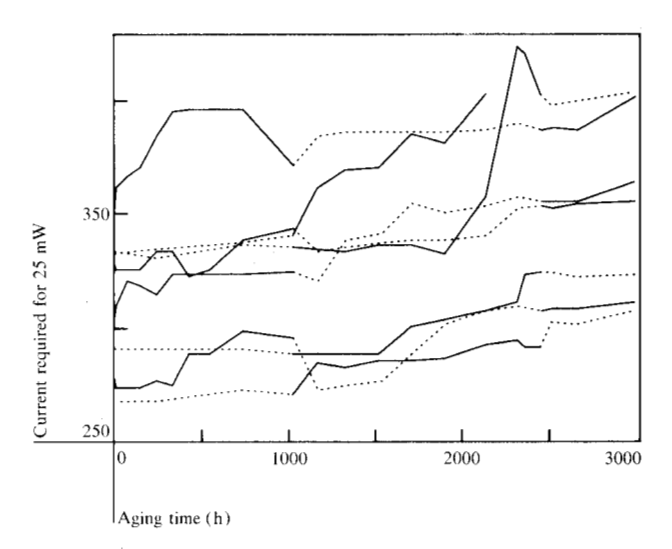


Figure 12 Constant-current aging at 25°C (solid lines) and 50°C (dashed lines). The current required for 25-mW output is measured at 25°C. Sharp degradation and subsequent annealing at 2400 hours in one unit are probably due to mechanical damage sustained by that laser.

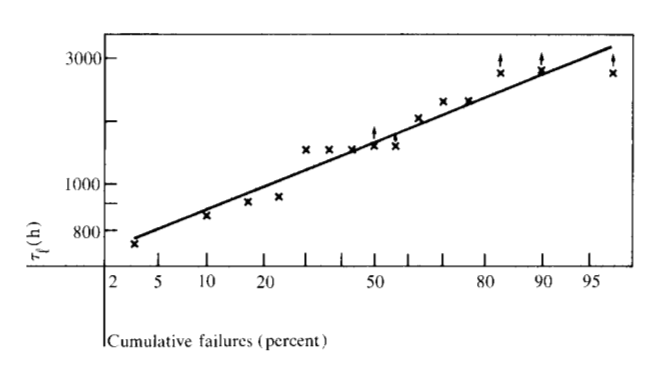


Figure 13 Log normal plot of laser lifetime vs cumulative failure percentage.

the time of failure of the first unit. A very long statistical average lifetime for individual lasers is not useful in this case if the observed distribution has a large standard deviation.

The lasers on life test were periodically checked for facet damage, and this was observed on several units (only the output facet was accessible in the package used). The time of appearance of this damage does not, however, generally correlate with changes in the degradation rate for that laser. The two remaining degradation modes observed in the present experiment are the development of kinks at 10 to 20 mW [57] and an increase in thermal resistance. These strongly reinforce each other,

raising the operating current and resulting in severe heating. Although degraded lasers often work very well in the power range up to about 5 mW, they are unable to reach 20 mW because of overheating. The increase in thermal resistance has been attributed to degradation of the solder contact between the chip and heat sink [42, 43]. The kink behavior during aging, in particular the ability of kinks to appear and disappear, is not yet understood. While neither of these degradation paths is unique to high-power operation, it seems that they both are strongly enhanced by the high current density and optical fields present. In particular, the bond degradation and resultant thermal runaway tend to widen the observed lifetime distribution compared to that expected for the same lasers run at lower current and output power. Fortunately, the simple screening used here identifies many of the early failures, leading to statistical lifetime figures that make these DH lasers, even though not yet optimized, very attractive for high-power cw applications.

Conclusion

Substantial progress has been made towards obtaining long-lived high-power cw semiconductor lasers on a reproducible basis. Many problems associated with liquid phase epitaxial growth have been identified and solved or minimized. Some interesting anomalous operating characteristics have been observed and explained. Much work remains, both in the fundamental physics of such things as degradation mechanisms and in the technology of commercial manufacturability. It seems clear, however, that the bright future predicted long ago for semiconductor lasers is now in sight.

Acknowledgments

It is a pleasure to acknowledge the able technical assistance of A. R. Benoric, C. B. Burstell, V. Garrison, H. C. Ifill, and R. M. Potemski. Some of the work described here was done in collaboration with L. Yang. We have also benefitted from discussions with our colleagues J. M. Ballantyne, L. D. Comerford, J. D. Crow, W. P. Dumke, R. A. Laff, E. G. Lean, J. C. Marinace, and F. Stern.

References and note

- R. N. Hall, G. E. Fenner, J. D. Kingsley, T. J. Soltys, and R. O. Carlson, *Phys. Rev. Lett.* 9, 366 (1962).
- M. I. Nathan, W. P. Dumke, G. Burns, F. H. Dill, and G. Lasher, Appl. Phys. Lett. 1, 62 (1962).
- 3. T. M. Quist, R. H. Rediker, R. J. Keyes, W. E. Krag, B. Lax, A. L. McWhorter, and H. J. Zeigler, *Appl. Phys. Lett.* 1, 91 (1962).
- 4. H. Kroemer, Proc. IEEE 51, 1782 (1963).
- 5. H. Nelson, RCA Rev. 24, 603 (1963).
- 6. J. M. Woodall, H. Rupprecht, and G. D. Pettit, *IEEE Trans. Electron Devices* ED-14, 630 (1967).
- Z. I. Alferov, V. M. Andreev, D. Z. Garbuzov, Y. V. Zhilyaev, E. P. Morozov, E. L. Portnoi, and V. G. Trofim, Sov. Phys.—Semicond. 4, 1573 (1971) [Transl. of Fiz. Tekh. Poluprovodn. 4, 1826 (1970)].

- 8. I. Hayashi, M. B. Panish, P. W. Foy, and S. Sumski, *Appl. Phys. Lett.* 17, 109 (1970).
- 9. J. C. Dyment, Appl. Phys. Lett. 10, 84 (1967).
- J. C. Dyment, L. A. D'Asaro, J. C. North, B. I. Miller, and J. E. Ripper, *Proc. IEEE* 60, 726 (1972).
- J. M. Blum, J. C. McGroddy, P. G. McMullin, K. K. Shih, A. W. Smith, and J. F. Ziegler, *IEEE J. Quantum Electron*. QE-11, 413 (1975).
- 12. T. G. Giallorenzi, Proc. IEEE 66, 744 (1978).
- V. I. Bobrinev, V. S. Vorovev, Y. K. Kagan, M. A. Maiorchuk, A. L. Mikaelyam, and N. B. Nifantov, *Avtometriya*, No. 5, 52 (1977).
- 14. J. P. J. Heemskerk, Appl. Opt. 17, 2007 (1978).
- Y. Tsunoda, S. Sawano, H. Nakamura, K. Saito, T. Tsukada, and Y. Takeda, *IEEE Trans. Consum. Electron.* CE-23, 479 (1977).
- 16. A. J. Dewey, Proc. SID 19, 1 (1978).
- B. C. DeLoach, B. W. Hakki, R. L. Hartman, and L. A. D'Asaro, *Proc. IEEE* 61, 1042 (1973).
- 18. I. Ladany and H. Kressel, Appl. Phys. Lett. 25, 708 (1974).
- N. Chinone, H. Nakashima, and R. Ito, J. Appl. Phys. 48, 1160 (1977).
- R. L. Hartman, N. E. Schumaker, and R. W. Dixon, Appl. Phys. Lett. 31, 756 (1977).
- 21. H. Kressel and J. K. Butler, Semiconductor Lasers and Heterojunction LEDS, Academic Press, Inc., New York, 1977.
- 22. H. C. Casey and M. B. Panish, Heterostructure Lasers, Academic Press, Inc., New York, 1978.
- H. Yonezu, I. Sakuma, K. Kobayashi, T. Kamejima, M. Ueno, and Y. Nannichi, Jpn. J. Appl. Phys. 12, 1585 (1973).
- C. J. Neuse, H. Kressel, and I. Ladany, J. Vac. Sci. Technol. 10, 772 (1973).
- A. A. Berg and P. J. Dean, Light Emitting Diodes, Clarendon Press, Oxford, 1976, p. 392.
- 26. G. B. Stringfellow and R. T. Hall, J. Cryst. Growth 43, 47 (1976).
- R. D. Dupuis and P. D. Dapkus, Appl. Phys. Lett. 31, 466 (1977).
- B. I. Miller, J. H. Mcfee, R. J. Martin, and P. K. Tien, Appl. Phys. Lett. 33, 44 (1978).
- M. B. Panish and M. Ilegems, in *Progress in Solid State Chemistry*, Vol. 7, Pergamon Press, Elmsford, NY, 1972, p. 9.
- 30. J. M. Woodall, J. Cryst. Growth 12, 32 (1972).
- 31. I. Crossley and M. B. Small, J. Cryst. Growth 15, 275 (1972).
- 32. M. B. Small and R. Ghez, J. Appl. Phys. (in press).
- 33. E. A. Giess, J. D. Kuptsis, and E. A. D. White, *J. Cryst. Growth* 16, 36 (1972).
- 34. M. B. Small and I. Crossley, J. Cryst. Growth 27, 35 (1974).
- 35. M. B. Small and R. M. Potemski, J. Cryst. Growth 37, 163 (1977).
- 36. M. B. Small and R. Ghez, J. Cryst. Growth 43, 512 (1978).
- 37. G. R. Woolhouse, Phil. Mag. 36, 596 (1977).
- 38. E. Bauser, Appl. Phys. 15, 243 (1978).
- A. J. Springthorpe, F. D. King, and A. Beke, J. Electron. Mater. 4, 101 (1975).
- T. Fujiwara, K. Fujiwara, H. Ishikawa, M. Morimoto, and K. Hori, presented at the IEEE International Semiconductor Laser Conference, San Francisco, CA, 1978.
- J. D. Crow, L. D. Comerford, J. S. Harper, M. J. Brady, and R. A. Laff, Appl. Opt. 17, 479 (1978).
- 42. W. B. Joyce and R. W. Dixon, J. Appl. Phys. 46, 855 (1975).
- R. A. Laff, L. D. Comerford, J. D. Crow, and M. J. Brady, Appl. Opt. 17, 778 (1978).
- R. T. Lynch, Jr., L. Yang, and R. Y. Hung, *Electron. Lett.* 14, 769 (1979).
- 45. F. Stern, IEEE J. Quantum Electron. QE-2, 290 (1973).
- W. P. Dumke and J. M. Woodall, U.S. Patent 3,893,044, 1975; T. Tsukada, J. Appl. Phys. 45, 4899 (1974).
- D. V. Lang, R. L. Hartman, and N. E. Schumaker, J. Appl. Phys. 47, 4986 (1976).

- 48. R. T. Lynch, Jr., M. B. Small, and R. Y. Hung, Appl. Phys. Lett. 34, 297 (1979).
- 49. B. W. Hakki and F. R. Nash, J. Appl. Phys. 45, 3907 (1974).
- R. L. Hartman and R. W. Dixon, Appl. Phys. Lett. 26, 239 (1975).
- H. Ishikawa, T. Fujiwara, K. Fujiwara, M. Morimoto, and M. Takusagawa, J. Appl. Phys. (in press).
- O. Nakada, N. Chinone, S. Nakamura, H. Nakashima, and R. Ito, *Jpn. J. Appl. Phys.* 13, 1485 (1974).
- 53. H. Kressel and I. Ladany, RCA Rev. 36, 230 (1975).
- H. Yonezu, T. Yuasa, T. Shinohara, T. Kamejima, and I. Sakuma, *Jpn. J. Appl. Phys.* 15, 2393 (1976).
- H. Kressel, M. Ettenberg, and I. Ladany, Appl. Phys. Lett. 32, 305 (1978).
- S. Ritchie, R. F. Godfrey, B. Wakefield, and D. H. Newman, J. Appl. Phys. 49, 3127 (1978).
- 57. The lasers in the aging experiments described here generally are 250 to 500 μ m long. Although the shorter units have better *P-I* curve linearity, the degradation rate increases with decreasing length. This is possibly related to the increase in operating current density required to reach a particular output power in shorter lasers.

Received February 12, 1979; revised May 1, 1979

The authors are located at the IBM Thomas J. Watson Research Center, Yorktown Heights, New York 10598.